

The ¹²CO₂ and ¹³CO₂ Absorption Bands as Tracers of the Thermal History of Interstellar Icy Grain Mantles

JIAO HE,^{1,2} SM EMTIAZ,¹ ADWIN BOOGERT,³ AND GIANFRANCO VIDALI¹

¹*Physics Department, Syracuse University, Syracuse, NY 13244, USA*

²*Current address: Raymond and Beverly Sackler Laboratory for Astrophysics, Leiden Observatory, Leiden University, PO Box 9513, 2300 RA Leiden, The Netherlands*

³*Institute for Astronomy, University of Hawai'i at Manoa, 2680 Woodlawn Drive, Honolulu, HI 968221839, USA*

(Received January 1, 2018; Revised January 7, 2018; Accepted January 7, 2018)

Submitted to ApJ

ABSTRACT

Analyses of infrared signatures of CO₂ in water dominated ices in the ISM can give information on the physical state of CO₂ in icy grains and on the thermal history of the ices themselves. In many sources, CO₂ was found in the “pure” crystalline form, as signified by the splitting in the bending mode absorption profile. To a large extent, pure CO₂ is likely to have formed from segregation of CO₂ from a CO₂:H₂O mixture during thermal processing. Previous laboratory studies quantified the temperature dependence of segregation, but no systematic measurement of the concentration dependence of segregation is available. In this study, we measured both the temperature dependence and concentration dependence of CO₂ segregation in CO₂:H₂O mixtures, and found that no pure crystalline CO₂ forms if the CO₂:H₂O ratio is less than 23%. Therefore the segregation of CO₂ is not always a good thermal tracer of the ice mantle. We found that the position and width of the broad component of the asymmetric stretching vibrational mode of ¹³CO₂ change linearly with the temperature of CO₂:H₂O mixtures, but are insensitive to the concentration of CO₂. We recommend using this mode, which will be observable towards low mass protostellar envelopes and dense clouds with the James Webb Space Telescope, to trace the thermal history of the ice mantle, especially when segregated CO₂ is unavailable. We used the laboratory measured ¹³CO₂ profile to analyze the ISO-SWS observations of ice mantles towards Young Stellar Objects, and the astrophysical implications are discussed.

Keywords: astrochemistry — ISM: molecules — methods: laboratory: solid state — methods: laboratory: molecular

1. INTRODUCTION

CO₂ is abundant in quiescent and star-forming molecular clouds where it is found in ices with abundance in the 10 to 50% range with respect to water. Solid state CO₂ is mostly detected in the mid-infrared absorption through the asymmetric stretching mode ν_3 at ~ 2350 cm⁻¹ (Gerakines et al. 1999; Nummelin et al. 2001; Noble et al. 2013) and through the bending mode at

~ 665 cm⁻¹ (Gerakines et al. 1999; Pontoppidan et al. 2008; Ioppolo et al. 2013; Noble et al. 2013). Additional modes are detected as well, such as the combination modes $\nu_1 + \nu_3$ at 3708 cm⁻¹ and $2\nu_2 + \nu_3$ at 3600 cm⁻¹ (Gerakines et al. 1999; Keane et al. 2001). Unlike CO, which only has a high abundance in highly shielded regions, CO₂ has the same threshold of formation as water (Bergin et al. 2005; Whittet et al. 2009), which means that CO₂ is mixed with water in pristine polar ices coating dust grains (Whittet et al. 2009). The column density ratio of CO₂:H₂O varies between 10% and 50%, depending on the specific cloud. Laboratory measurements of CO₂-containing ice mixtures have found that the infrared absorption profile of CO₂ strongly depends on the physical and chemical environment in the

Corresponding author: Jiao He
jhe08@syr.edu

Corresponding author: Gianfranco Vidali
gvidali@syr.edu

ice, such as the temperature and the ice compositions (Gerakines et al. 1999; Öberg et al. 2009; Hodyss et al. 2008; He & Vidalí 2018). This makes CO₂ a very good candidate to trace the composition and physical condition of the ice mantle.

Since the ν_3 asymmetric stretch is particularly strong and often saturated, the ν_2 bending mode at ~ 650 cm⁻¹ and the ¹³CO₂ asymmetric stretching mode at ~ 2280 cm⁻¹ are often used instead to study CO₂ in ice mantles. So far, most of the observations of solid state CO₂ are through the 650 cm⁻¹ feature. Pontoppidan et al. (2008) used Spitzer to systematically study the 650 cm⁻¹ feature in Young Stellar Objects (YSOs). By comparing the observed absorption profile with laboratory measurements of different CO₂-containing ice mixtures, they found that the observed spectra can be fit well using five different components, each representative of CO₂ in different ice mixtures measured in the laboratory. However, there are redundancies in the derived ice compositions that are further amplified by the effect of the poorly constrained grain shapes on the observed spectral profiles. The latter is not the case for ¹³CO₂ because it is diluted by almost two orders of magnitude in the ice, resulting in a low polarizability and thus negligible grain shape effects (Boogert et al. 2000). Therefore, the observed ¹³CO₂ spectra can be readily compared with laboratory measured spectra. Its asymmetric stretching feature cannot be observed with ground-based telescopes because of strong telluric absorption. The only comprehensive study of this feature is by Boogert et al. (2000) who used ISO-SWS to observe ¹³CO₂ in 13 sightlines. However, due to limited sensitivity, only a small sample of sightlines could be observed, lacking in particular the envelopes of low mass YSOs and quiescent dense molecular clouds. The forthcoming James Webb Space Telescope (JWST) is expected to cover this spectral region at orders of magnitude better sensitivity and somewhat higher spectral resolution ($R = \lambda/\Delta\lambda \sim 3000$ versus 2000). A comprehensive set of laboratory measurements of solid state ¹³CO₂ would facilitate the interpretation of JWST observations of solid CO₂. One of the motivations of this work is to measure the absorption profile of ¹³CO₂ ν_3 mode in CO₂:H₂O mixtures at different mixing ratios and different temperatures, providing improved insights into the composition as well the thermal history of interstellar and circumstellar icy mantles.

In some of the sightlines observed by Pontoppidan et al. (2008) and Gerakines et al. (1999), the CO₂ bending profile shows double splitting features. This is interpreted as the Davydov splitting—which occurs in crystals with more than one identical molec-

ular species or unit per unit cell. It is commonly interpreted as an indication of “pure” crystalline CO₂ (Pontoppidan et al. 2008; Isokoski et al. 2013; Cooke et al. 2016; Baratta & Palumbo 2017). Since ices in the ISM are water-dominated, the appearance of the splitting indicates the formation of segregated CO₂ solids due to thermal processing. Öberg et al. (2009) measured the temperature dependence of the segregation of CO₂ from CO₂:H₂O mixtures. The majority of their experiments were carried out with a CO₂:H₂O mixing ratio of 1:2, with only one measurement for 1:4, a more representative ratio for the ices coating grains (Boogert et al. 2015). From an Arrhenius fitting to the experimental data, they found an energy barrier of 1090 ± 15 K for segregation of CO₂. This translates in a segregation temperature of 30 ± 5 K, assuming a segregation time scale of 4000 yrs. He et al. (2017) obtained an onset of segregation of CO₂ on the surface of non-porous Amorphous Solid Water (np-ASW) at 65 K, corresponding to a temperature in space of 43 ± 3 K, assuming a diffusion pre-exponential factor of 10^{12} s⁻¹ and a similar segregation time scale as in Öberg et al. (2009). This temperature range is somewhat higher than the result of Öberg et al. (2009).

Since CO₂ is present in a wide range of concentrations with respect to water in ices (Boogert et al. 2015; Yamagishi et al. 2015), in order to correctly interpret IR spectra for studying the thermal evolution of ices, it is necessary to know how the level of CO₂ concentration in mixed CO₂:H₂O ices impacts segregation. In this work, we comprehensively study the concentration dependence as well as temperature dependence of CO₂ segregation from CO₂:H₂O mixtures. In a previous work (He & Vidalí 2018), we found that the $\nu_1 + \nu_3$ mode at ~ 3708 cm⁻¹ and the $\nu_1 + 2\nu_2$ mode at ~ 3600 cm⁻¹ provide useful tools to quantify CO₂ segregation in laboratory measurements. In this work, we study the profiles of the combination modes and show that they can be used to assess the degree of order of CO₂ in CO₂:H₂O ices. To obtain the thermal history of a CO₂:H₂O ice and to compare it with spectra obtained with the ISO-SWS, we use the ν_3 absorption profile of ¹³CO₂ naturally occurring in laboratory CO₂:H₂O ice mixtures.

The remaining of this paper is organized as follows: Section 2 describes the experimental setup, followed by Section 3 on results and analysis. Section 4 compares our laboratory measured spectra of ¹³CO₂ with ISO-SWS data and discusses the astrophysical implications.

2. EXPERIMENTAL SETUP

Experiments were carried out in a ultra-high vacuum (UHV) apparatus at Syracuse University. The UHV

chamber is pumped by a combination of turbopumps and a cryopump. After bake-out, the base pressure reaches 4×10^{-10} Torr routinely. At the center of the UHV chamber, a gold-coated copper disc was used as the sample. The sample can be cooled down to 5 K by an Advanced Research Systems DE-204S cryocooler, or heated up to room temperature using a cartridge heater located right behind the sample. The sample temperature was measured by a calibrated silicone diode to an accuracy better than 50 mK. A Lakeshore 336 temperature controller was used to read and control the temperature.

The IR spectra of ices deposited on the sample were recorded using a Nicolet 6700 Fourier Transform Infrared (FTIR) in the Reflection Absorption Infrared Spectroscopy (RAIRS) configuration with an incident angle of ~ 78 degrees. The FTIR collects and averages 9 spectra every 20 seconds at a resolution of 0.5 cm^{-1} in the range of $600\text{--}4000 \text{ cm}^{-1}$. Because of the strong signals, we took averages of fewer scans than it is typically done in order to obtain a good time resolution during warming up of the ice sample. The heating ramp rate during temperature programmed desorption (TPD) was 0.1 K/s (except for dedicated flash heatings), which amounts to one infrared spectrum every 2 K. The modalities of deposition of $\text{CO}_2\text{:H}_2\text{O}$ mixtures onto the gold-plated copper sample are discussed in the Appendix.

3. RESULTS AND ANALYSIS

We carried out three sets of experiments. In the first set, we study the temperature dependence of IR absorption bands of $\text{CO}_2\text{:H}_2\text{O}$ mixtures of different mixing ratios as they were heated linearly from 10 K to 200 K. In the second set, we fix the $\text{CO}_2\text{:H}_2\text{O}$ ratio and carried out isothermal experiments at different temperatures to find out the temperature at which CO_2 segregation maximizes. A higher temperature facilitates segregation, but at too high a temperature, CO_2 desorption begins to compete with segregation. There should exist an optimum temperature that maximizes segregation. In the third set of experiments, we fix the temperature for the isothermal experiments at the temperature of maximum segregation we found from the second set of experiments, and check how segregation depends on CO_2 concentration.

3.1. Temperature dependence of IR bands

In this set of experiments, 50 ML of water and various amount of CO_2 were co-deposited on the sample at 10 K, to make the following $\text{CO}_2\text{:H}_2\text{O}$ mixtures: 5:100, 10:100, 15:100, 20:100, 25:100, 30:100, 40:100, and 50:100. After

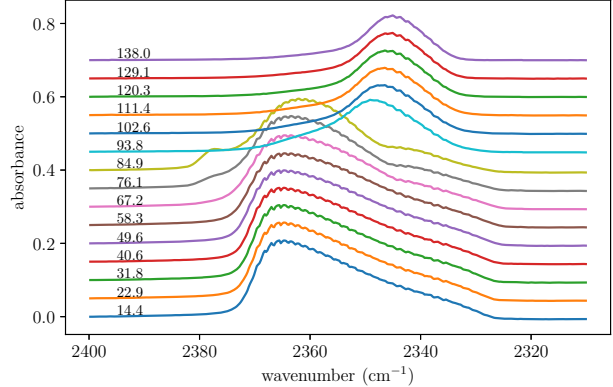


Figure 1. RAIRS of ν_3 band of 50:100 $\text{CO}_2\text{:H}_2\text{O}$ mixture deposited at 10 K and heated at 0.1 K/s. The temperature of each curve is marked. The small oscillations superimposed on the curves are due to gas-phase CO_2 in the spectrometer.

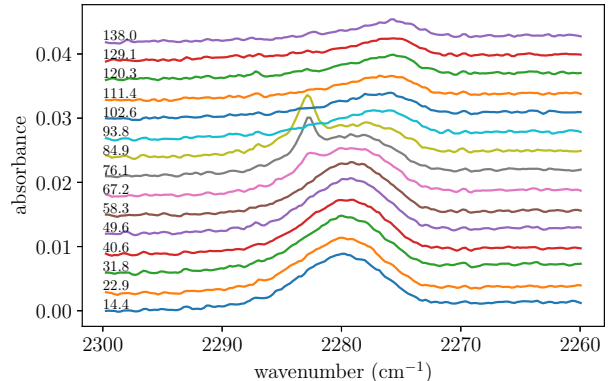


Figure 2. Same as Figure 1, but for the ν_3 band of $^{13}\text{CO}_2$ that is present in natural abundance in $\text{CO}_2\text{:H}_2\text{O}$ ice mixtures.

deposition, the ice mixtures were heated linearly from 10 K to 200 K at 0.1 K/s. Figures 1, 2, and 3 show the absorption bands ν_3 , $^{13}\text{CO}_2 \nu_3$, and the combination modes of a 50:100 $\text{CO}_2\text{:H}_2\text{O}$ mixture at selected temperatures during heating. Figure 4 shows the integrated band area of the ν_3 peak at around 2350 cm^{-1} for $\text{CO}_2\text{:H}_2\text{O}$ mixtures of different mixing ratios during the heating up.

The $\text{CO}_2 \nu_3$ mode shows an asymmetric peak centered at about 2365 cm^{-1} at low temperatures. He & Vidali (2018) has shown that the ν_3 peak of CO_2 on water ice surface is dependent on the CO_2 coverage. As the coverage increases from zero to more than 2 layers (L), the peak shifts from $\sim 2347 \text{ cm}^{-1}$ to $\sim 2376 \text{ cm}^{-1}$. The shape and position of the spectra in Figure 1 at low temperatures are qualitatively similar to the submonolayer spectra shown in Figure 1 of He et al. (2017). As the ice

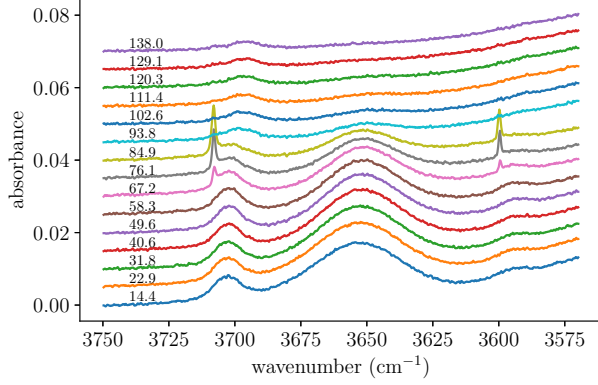


Figure 3. Same as Figure 1, but for the 3570 cm^{-1} to 3750 cm^{-1} range.

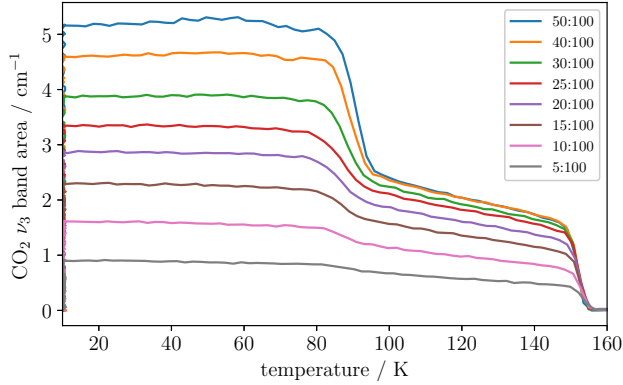


Figure 4. Band area of the ν_3 absorption peak of CO_2 during warming up of the $\text{CO}_2\text{:H}_2\text{O}$ mixtures with different mixing ratios (see inset).

is heated to the 70–80 K range, a peak at $\sim 2378 \text{ cm}^{-1}$ emerges, which is a signature of “pure” crystalline form of CO_2 after segregation has taken place. Between 80 and 100 K, the ν_3 band area of CO_2 decreases. This is due to the desorption of weakly bound CO_2 on the surface of water ice (including the surface of pores). The remaining CO_2 molecules that are trapped inside the water ice matrix have an absorption peak at around 2345 cm^{-1} that redshifts with temperature. Between 100 K and 150 K, the CO_2 amount decreases linearly with temperature. This slow desorption is induced by the compaction of ASW, and CO_2 molecules are pushed out of the water matrix during the pore collapse of ASW. Between 150 K and 155 K, water crystallizes and all of the remaining CO_2 desorb from the ice. This is referred to as the “molecular volcano desorption” (Smith et al. 1997).

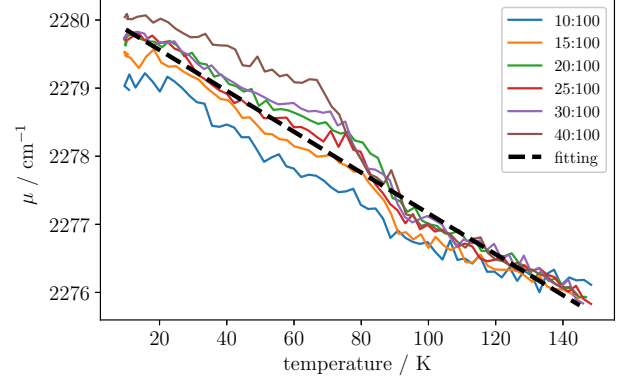


Figure 5. Center position (μ) of the Gaussian disordered component of the $^{13}\text{CO}_2$ ν_3 absorption peak at $\sim 2280 \text{ cm}^{-1}$ for different ratios of $\text{CO}_2\text{:H}_2\text{O}$ mixtures during warm-up. The $\text{CO}_2\text{:H}_2\text{O}$ ratio is in the inset.

A similar trend is also seen in the ν_3 $^{13}\text{CO}_2$ band. When CO_2 segregates, a peak at 2282 cm^{-1} emerges. This peak is characteristic of $^{13}\text{CO}_2$ with natural isotopic abundance (He et al. 2017), and is more sensitive to segregation than the ν_3 peak of CO_2 at around 2376 cm^{-1} . During the heating from 10 K to 140 K, the peak red shifts from about 2280 cm^{-1} to about 2276 cm^{-1} , and the width becomes narrower with temperature. To see more clearly how the peak position and width change with temperature, we used one broad Gaussian lineshape and one narrow Lorentzian lineshape to fit $^{13}\text{CO}_2$ in disordered and ordered (crystalline) CO_2 , respectively. Although the disordered component has an asymmetric shape, for simplicity we still use a Gaussian function. This fitting scheme is sufficient to reliably obtain the peak position and the width. Figure 5 and 6 show the center position (μ) and the $FWHM$ of the Gaussian fit, respectively. Both the center position μ and $FWHM$ decrease with temperature roughly linearly. The best fitting parameters with a 95% confidence interval are

$$\mu = (2280.16 \pm 0.06) - (0.030 \pm 0.0006)T \quad (1)$$

$$FWHM = (8.6 \pm 0.7) - (0.022 \pm 0.001)T \quad (2)$$

where the unit is cm^{-1} for μ and $FWHM$, and Kelvin for T . These simple functions will be useful for the analysis of the observed $^{13}\text{CO}_2$ profile, to be discussed below.

Figure 3 shows the region of the $\nu_1 + \nu_3$ $^{12}\text{CO}_2$ mode at around 3700 cm^{-1} , $\nu_1 + 2\nu_2$ $^{12}\text{CO}_2$ mode at 3600 cm^{-1} , as well as a peak at $\sim 3650 \text{ cm}^{-1}$. The 3650 cm^{-1} peak can be attributed to $^{12}\text{CO}_2$ on the surface of water. This feature is common in $\text{CO}_2\text{:H}_2\text{O}$ mixtures or CO_2 on the surface of water at low temperatures. The $\nu_1 + \nu_3$ and $\nu_1 + 2\nu_2$ combination modes are broad at low tempera-

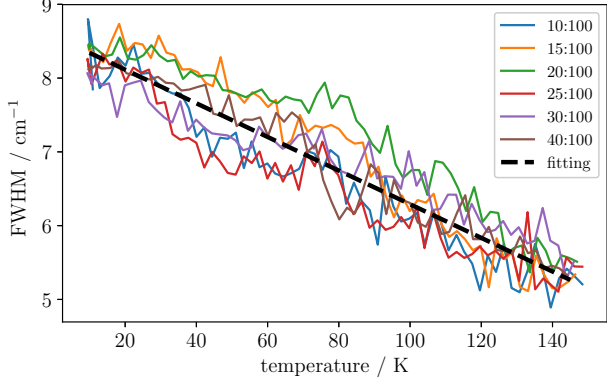


Figure 6. Same as in Figure 5 but for *FWHM*.

tures. As the CO_2 segregates, a sharp feature emerges for both combination modes. After weakly bound CO_2 has desorbed from the surface, the 3600 cm^{-1} peak is barely seen, but the peak at 3700 cm^{-1} is still clearly visible. Its position and width are no different from the 3-coordinated dangling bond of amorphous water annealed at similar temperatures. We attribute this peak to the dangling bond of ASW, although we do not exclude the possibility that the $\nu_1 + \nu_3$ mode of CO_2 may also have a small contribution to this peak.

3.2. Segregation of CO_2 in $\text{CO}_2\text{:H}_2\text{O}$ mixtures

Prior laboratory measurements (Hodyss et al. 2008; He & Vidali 2018) have shown that the segregation and crystallization of CO_2 is accompanied by changes in the bending, asymmetric stretching (for both $^{12}\text{CO}_2$ and $^{13}\text{CO}_2$), and combination modes. The bending mode absorption at $\sim 650 \text{ cm}^{-1}$ is an important feature that is used to characterize CO_2 ice (Pontoppidan et al. 2008). Toward heavily embedded YSOs, the bending mode is easier to observe than the combination modes or the ν_3 of $^{13}\text{CO}_2$ because of the brighter continuum emission at $15 \text{ }\mu\text{m}$. However, the bending mode band is close to the lower limit of our infrared detector, and the signal is weak. Following our previous work on CO_2 ice (He & Vidali 2018), we use the $\nu_1 + \nu_3$ combination mode at around 3700 cm^{-1} to quantify the segregation. The analysis of segregation based on the combination mode at 3700 cm^{-1} should not differ from the that using the bending mode at $\sim 650 \text{ cm}^{-1}$.

We decompose the profile of the combination mode at $\sim 3700 \text{ cm}^{-1}$ into two components, one broad Gaussian component centered at $\sim 3703 \text{ cm}^{-1}$ attributed to disordered CO_2 , and one sharp Lorentzian component centered at 3708 cm^{-1} attributed to (poly)crystalline CO_2 . An example of the fitting is shown in Figure 7. We defined the “degree of crystallinity” (*DOC*) as the frac-

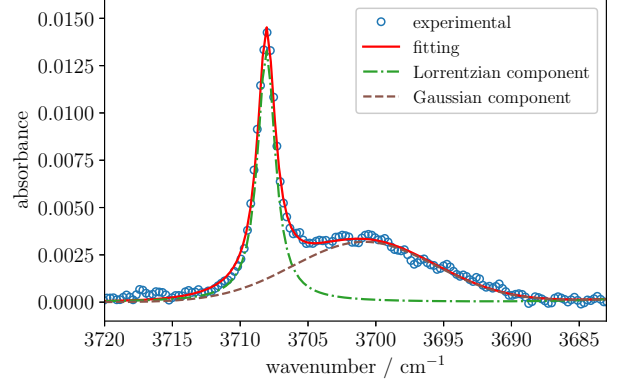


Figure 7. An example of fitting the CO_2 $\nu_1 + \nu_3$ mode absorption profile using a Lorentzian component and a Gaussian component.

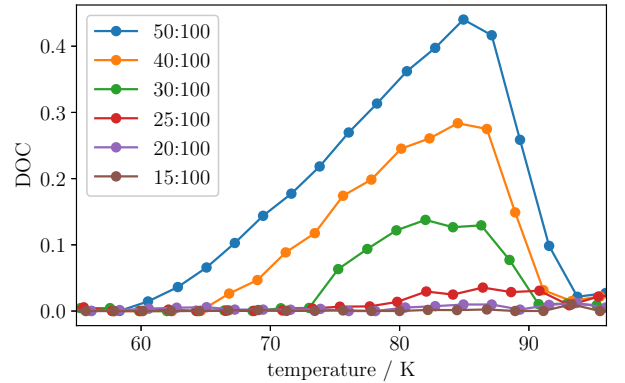


Figure 8. The degree of crystallinity (*DOC*) of $\text{CO}_2\text{:H}_2\text{O}$ mixtures when warming up the ice at a ramp rate of 0.1 K/s . The mixing ratios are shown in the figure.

tion of CO_2 in the (poly)crystalline form (the Lorentzian component).

$$DOC = \frac{A_{\text{crystalline}}}{A_{\text{crystalline}} + A_{\text{amorphous}}} \quad (3)$$

where $A_{\text{crystalline}}$ and $A_{\text{amorphous}}$ are the band area of the Lorentzian component and Gaussian component, respectively. We calculate *DOC* of the experiments presented in Section 3.1. The results are shown in Figure 8.

From Figure 8, it can be seen that the segregation strongly depends on both concentration and temperature. Here we did the experiments at a fixed heating ramp rate. It is possible that different ramp rates would also yield different segregation ratios. To use CO_2 segregation to trace the temperature history of the ice mantle would require a systematically study of the segregation over the whole parameter space of time, temperature,

and concentration, which is a very time consuming set of measurements. Here we take a simpler approach and focus on one parameter at a time. A set of isothermal experiments were devoted to find out the temperature that maximizes the segregation. We deposited 50 ML of water and 30 ML of CO_2 simultaneously onto the sample at 10 K, then flash heated the sample at a rate of 0.5 K/s to a target temperature and kept it at that temperature for 2 hours while monitoring the $\nu_1 + \nu_3$ mode. The band area of the Lorentzian component at different target temperatures as a function of time is shown in Figure 9. It can be seen that 72 K is the most favorable temperature to form crystalline CO_2 in $\text{CO}_2:\text{H}_2\text{O}$ mixtures. Below 72 K the mobility of CO_2 is not enough for segregation of CO_2 to occur to the fullest extent, while above 72 K the desorption of CO_2 starts to play a significant role. At 70 and 68 K, the segregated CO_2 does not reach maximum after 2 hours. To verify that the highest degree of segregation is indeed achieved at 72 K instead of 68 K or 70 K, we use a function to fit the curves and try to find the saturation level. Öberg et al. (2009) found that the segregation during isothermal experiments cannot be fit by a single exponential function. Two exponential functions are required to fit it. They attributed the two parts of the segregation to two distinct mechanisms of segregation—surface processes and bulk processes. Here we focus on the second part of the segregation only and use the function $a(1 - \exp(-bt)) + c$ to fit the 68–72 K curves after the first 10 minutes. The fitting are extrapolated to 4 hours to show the saturation level, from which it is clearly that 72 K is the favorable temperature that maximizes the segregation. Based on Figure 8, the temperature at which the DOC maximizes is similar for all concentrations. Therefore, it is fair to assume that this favorable temperature 72 K works for all concentrations.

After finding this most favorable isothermal experimental temperature, we fix the temperature and try different concentrations to obtain the lowest concentration required for the formation of “pure” crystalline CO_2 . We fixed the amount of water deposited at 50 ML and selected the CO_2 dose to be: 2.5, 5.0, 7.5, 10, 11.5, 12.5, 15, 20, and 25 ML. After the co-deposition at 10 K, the ice mixtures were heated to 72 K at a ramp rate of 0.5 K/s and then kept at 72 K for 2 hours. Figure 10 shows the DOC as a function of isothermal experimental time at different target temperatures. It can be seen that below the $\text{CO}_2:\text{H}_2\text{O}=23:100$ concentration, the DOC is almost zero. We thus conclude that 23% is the threshold concentration to obtain “pure” crystalline CO_2 in $\text{CO}_2:\text{H}_2\text{O}$ mixtures.

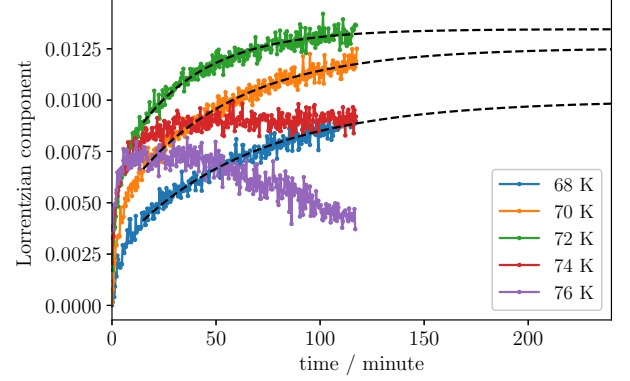


Figure 9. The band area of the Lorentzian component of $\nu_1 + \nu_3$ at 3708 cm^{-1} during isothermal experiment of a 30:100 $\text{CO}_2:\text{H}_2\text{O}$ mixture at different temperatures. The isothermal temperature is marked in the figure. The dashed lines are the fitting using a function $a(1 - \exp(-bt)) + c$.

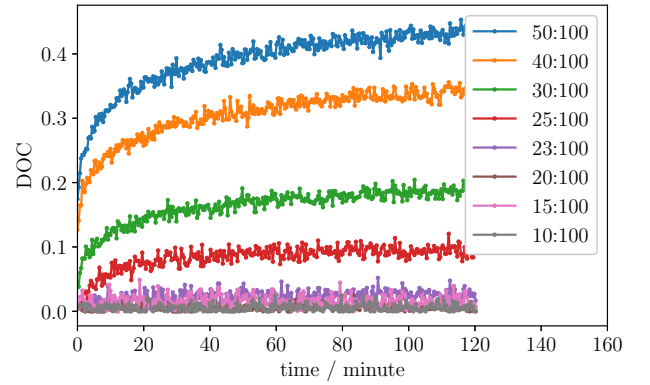


Figure 10. The degree of crystallinity (DOC) of $\text{CO}_2:\text{H}_2\text{O}$ mixture for different concentrations (see inset) during isothermal experiments at 72 K.

4. ASTROPHYSICAL IMPLICATIONS

4.1. $\text{CO}_2:\text{H}_2\text{O}$ ices as Temperature Tracers

CO_2 is one of the main components of ISM ice mantles. In some of the observed sightlines, CO_2 is in the “pure” crystalline form, as seen from the double splitting of the bending absorption profile. This splitting feature has been proposed to be a candidate tracer of the thermal history of the ice mantle. Prior laboratory studies (Ehrenfreund et al. 1999; Hodyss et al. 2008; Öberg et al. 2009) have found that the segregation of CO_2 from ice mixtures is a function of temperature, and the segregation is irreversible with temperature. Experiments in this work show that the segregation of CO_2 from a $\text{CO}_2:\text{H}_2\text{O}$ mixture is not only temperature dependent but also strongly affected by the

concentration of CO_2 . In fact, if the concentration of CO_2 is too low, pure crystalline CO_2 never forms, regardless of the thermal history. According to our measurements, the concentration threshold for CO_2 segregation is 23:100. This is larger than the average $\text{CO}_2/\text{H}_2\text{O}$ column density ratio observed toward massive YSOs ($17 \pm 3\%$; Gerakines et al. (1999)) and comparable to the $\sim 25\%$ ratio of the low mass YSOs (Pontoppidan et al. 2008). The segregated CO_2 detected in these sightlines (e.g., S140 IRS1) might thus probe $\text{CO}_2/\text{H}_2\text{O}$ concentrations that are enhanced at certain locations along the sightline or in certain ice layers.

Our experiments show that the $^{13}\text{CO}_2$ absorption profile at around 2280 cm^{-1} is a good tracer of the thermal history of the ice mantle, even if there is no sign of the very narrow feature of segregated crystalline CO_2 . Figure 5 and Figure 6 show that both the peak position (in cm^{-1}) and width decrease with increasing temperature, but they are not sensitive to CO_2 concentration. This isolates the effect of temperature from the effect of concentration, and thus provides an easy tool for the determination of the thermal history. Next we try to fit the $^{13}\text{CO}_2$ spectra in Boogert et al. (2000) based on our laboratory measurements. We visually examine the observed spectra and separate them into two groups: group 1 without a significant narrow blue peak at 2283 cm^{-1} , and group 2 with it. Spectra in group 1 are fit with a single Gaussian function, while spectra in group 2 are fit with one Gaussian function for disordered CO_2 and one Lorentzian function for crystalline CO_2 , as shown in Figure 11 and 12. The best fit peak position, full width at half maximum ($FWHM$) as well as the calculated temperature based on the Gaussian component using Equation 2 are also shown for each spectrum. For group 2, the magnitude of both components are also shown.

The temperatures quoted in Figure 11 and 12 are based on the laboratory time scale. In a typical astrophysically relevant time scale, the warming up of the ice is over a much longer time, and a lower temperature is expected to yield the same structural changes in the ice mixture. To translate the ice's temperature in the laboratory time scale T_{lab} to the temperature in astronomical conditions T_{ast} , an Arrhenius-type expression can be used to describe the rate of segregation.

$$k = \nu \exp(-E_{\text{seg}}/T) \quad (4)$$

where ν and E_{seg} are the prefactor and the energy barrier (in unit of degree Kelvin) for CO_2 segregation, respectively. The time scale for segregation to happen can be approximated by $t \sim k^{-1}$. The temperature at which

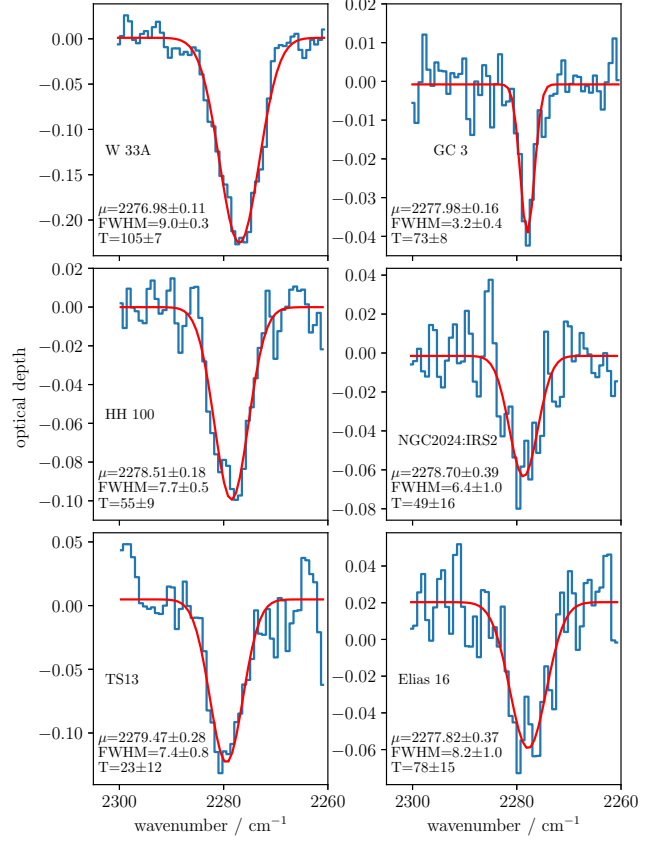


Figure 11. Fitting of selected ISO-SWS spectra of $^{13}\text{CO}_2$ using one Gaussian function. The fitting parameters are shown in the figure. The temperature T is calculated using Eq 1, and corresponds to the temperature in the laboratory time scale. To convert the time scale to that of the warming up stage of a interstellar clouds, the temperature should be multiplied by a factor of 0.3–0.5.

segregation happens most efficiently is:

$$T = \frac{E_{\text{seg}}}{\ln(\nu t)} \quad (5)$$

In laboratory experiments, the time scale t_{lab} is in the order of seconds. Under astronomical conditions, the free fall time between distances that have temperature of 70–90 K for a low mass star is 75 yrs (Pontoppidan et al. 2008). Rotation will slow down this process, but 10^2 – 10^3 yrs for the temperature range where segregation takes place is a reasonable estimate. The lifetime of hot cores around massive YSOs is 30,000 yrs (Charnley et al. 1992). These hot cores have temperatures exceeding 100 K, but there is a gradient outside of that where ices have not yet evaporated and are heated during that time. We adopt the range of 10^2 – 10^5 yrs for the segregation time scale under astronomical conditions. The conversion factor from laboratory time scale to astro-

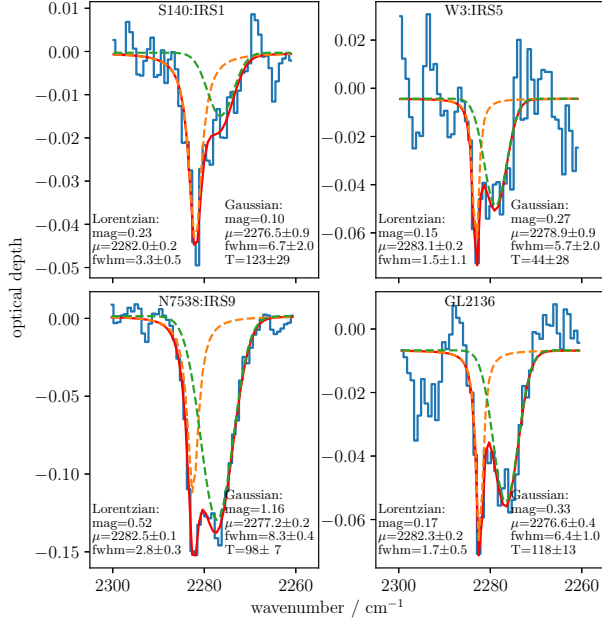


Figure 12. Fitting of selected ISO-SWS spectra of $^{13}\text{CO}_2$ using one Gaussian distribution and one Lorentzian distribution. The fitting parameters are shown in the figure. The temperature T refers to the laboratory time scale.

nominal time scale is:

$$\frac{T_{\text{ast}}}{T_{\text{lab}}} = \frac{\ln(\nu t_{\text{lab}})}{\ln(\nu t_{\text{ast}})} \quad (6)$$

The prefactor ν is not well characterized. Öberg et al. (2009) did isothermal experiments of 1:2 $\text{CO}_2:\text{H}_2\text{O}$ mixtures and reported a prefactor of $2 \times 10^{5 \pm 1} \text{ s}^{-1}$ for segregation. This prefactor likely reflects a combined effects of CO_2 diffusion on ASW and the collapse of pores in ASW. Using this prefactor, the conversion factor can be calculated to be in the 0.3–0.4 range. If we assume that the segregation is dominated by the diffusion of CO_2 on the pore surface of ASW and take the laboratory determined prefactors for volatile molecules such as CO, N_2 , CH_4 , which are mostly in the $10^{8 \pm 1}$ range (He et al. 2018), then the conversion factor is in the 0.4–0.5 range. In summary, to convert the temperature in the laboratory time scale to that of the warming up of a interstellar cloud, a factor 0.4 ± 0.1 should be considered. With a correction for time scale taken into account, the dependence of segregation on both concentration and temperature shown in Figure 8 should be useful in models of YSO envelopes.

4.2. Comparison with Astronomical Spectra

In the sightline of W33A, the $^{13}\text{CO}_2$ absorption peak is centered at 2277 cm^{-1} , which corresponds to a temperature of 105 K in the laboratory time scale. But if we

plug $T = 105 \text{ K}$ into Eq 2, the calculated $FWHM = 6.3 \text{ cm}^{-1}$ is much smaller than that for the observed one 9.0 cm^{-1} . Note that this is likely not due to contamination by CO mixed in the ices, because W33A has less contribution from CO (10%) compared to other YSOs, e.g., NGC 7538 IRS9 (20%; Pontoppidan et al. (2008)). This inconsistency is likely due to the non-uniform temperature along the sightline. For this reason, we use the peak position in Eq 1 instead of the $FWHM$ in Eq 2 to determine the temperature. In general, the best fit temperature in Figure 11 should be understood as the average temperature along the sightline.

So far, we used CO_2 in water ice to obtain the temperature of the ice. Now we put the temperature traced by $^{13}\text{CO}_2$ in the context of the observed sightlines. Of the targets with a single “disordered” $^{13}\text{CO}_2$ component (Figure 11), the peak of R CrA IRS2 (TS13) has the largest wavenumber, and thus the lowest temperature. The space temperature of $(0.4 \pm 0.1) \times (23 \pm 12) \text{ K}$ is well below that for CO sublimation, and indeed this sightline harbors an exceptionally large apolar CO component (Vandenbussche et al. 1999). The two other high quality spectra of the low mass YSO HH 100 IR and the massive YSO W33A show $^{13}\text{CO}_2$ bands peaking at smaller wavenumbers, corresponding to space temperatures of $(0.4 \pm 0.1) \times (55 \pm 9) \text{ K}$ and $(0.4 \pm 0.1) \times (105 \pm 7) \text{ K}$, respectively. Indeed, the CO profile of W33A is dominated by polar CO ices (Pontoppidan et al. 2003), indicating that the volatile apolar CO ices have sublimated, and a significant abundance of warm CO gas is detected in this sightline (Mitchell et al. 1990). The relatively high $^{13}\text{CO}_2$ temperature for HH 100 seems puzzling considering the large abundance of apolar CO (Pontoppidan et al. 2003). This likely reflects a large temperature gradient in the HH 100 YSO envelope, with colder apolar CO dominating the ices at larger radii. One should also consider the possibility that the $\text{CO}_2:\text{H}_2\text{O}$ ices are formed earlier in the cloud history in less shielded conditions on warmer grains than the volatile CO. Then the $^{13}\text{CO}_2$ profile reflects the formation temperature. This can be tested by observations towards background stars tracing quiescent clouds. Unfortunately, the ISO/SWS spectrum of Elias 16, a background star of the Taurus Molecular Cloud, is of low quality, but will be vastly improved when observed with JWST in the near future. For a discussion regarding the targets with segregated crystalline $^{13}\text{CO}_2$ (Figure 12) we refer to Boogert et al. (2000) and van der Tak et al. (2000), who show that the degree of segregation correlates with the dust temperature as the YSO envelope becomes less massive and hotter over time scales of a few times 10,000 yrs.

In the second group (Figure 12), we used one broad Gaussian and one narrow Lorentzian to fit the spectra. The temperatures are derived from the broad component using Eq 1. Boogert et al. (2000) used a narrow Gaussian instead of a Lorentzian to fit the 2283 cm^{-1} feature. They found that the narrow feature is present only toward high mass protostars, even though not all high mass protostars have the narrow feature (see Boogert et al. (2000) for a detailed discussion). In these four sightlines, the temperatures are all relatively high, in agreement with the previous proposition that segregation indicates thermal processing. Because of more free parameters being used in the fitting, the uncertainty in temperature is much larger than in group 1. Furthermore, the signal-to-noise ratios of the spectra from S140:IRS1 and W3:IRS5 are not good enough for an accurate determination of the peak position of the disordered component. To better constrain the temperature would require better signal-to-noise ratio of the spectra. The James Webb Space Telescope (JWST) is expected to cover these regions at orders of magnitude better sensitivity and somewhat larger spectral resolution ($R = 3,000$ versus $2,000$), and more accurate temperature determination and sorting of features between different classes of objects will be possible. The bending mode profile at $15\text{ }\mu\text{m}$ can also be used as a supplementary tool to further constrain the temperature.

Previously, Boogert et al. (2000) compared the observed spectra with the laboratory measurement of Ehrenfreund et al. (1999). They found a similar redshift and a narrowing of the $^{13}\text{CO}_2$ peak as the temperature of the $\text{CO}_2:\text{H}_2\text{O}$ mixture was increased. They also found that during heating a $1:0.92:1\text{ H}_2\text{O}:\text{CH}_3\text{OH}:\text{CO}_2$ mixture, the peak position and width changed, but with a different temperature dependence than that of a $\text{CO}_2:\text{H}_2\text{O}$ mixture. Therefore, Boogert et al. (2000) concluded that while $^{13}\text{CO}_2$ traces segregation, it is not suitable for temperature determinations, because the temperature effect could not be separated from composition effects. In their experiment, the concentration of CH_3OH is much higher than what is typically observed. CH_3OH is formed mostly on dust grains by the consecutive hydrogenation of CO after the heavy CO freeze-out. This formation mechanism is corroborated by both laboratory measurements (Hama & Watanabe 2013) and observations (Boogert et al. 2011), which show that CH_3OH is mostly found in high extinction regions. Conversely, CO_2 is mostly found in a water-rich environment, consistent with the scenario that CO_2 is formed together with water. Although most recent laboratory experiments found that CH_3OH can also be formed before the heavy freeze-out of CO by the reaction

between CH_3 and OH (Qasim et al. 2018), the question still remains of how much CH_3OH can be formed this way. Based on the current state of knowledge, it is safe to assume that CO_2 mostly interacts with water instead with CH_3OH in the ice, and therefore it is justifiable to ignore the effect of CH_3OH on the $^{13}\text{CO}_2$ absorption profile.

4.3. $\text{CO}:\text{CO}_2$ Ices

This assumption seems less applicable to CO mixed in the ices. Previous analysis of the CO_2 bending mode absorption profile at $15\text{ }\mu\text{m}$ and the blue component of CO absorption profile at $4.7\text{ }\mu\text{m}$ reveals that 10-30% of the CO_2 molecules are mixed with CO (Pontoppidan et al. 2008, 2003). This group proposed that “pure” crystalline CO_2 can be formed either by thermally-induced CO_2 segregation from a $\text{CO}_2:\text{H}_2\text{O}$ mixture, or by CO desorption from a $\text{CO}:\text{CO}_2$ mixture. The mechanism of segregation is closely related to the mechanism of CO_2 formation. So far there are mainly two categories of mechanisms proposed to explain the formation of CO_2 molecules on grains. The first category involves pure thermal reactions among CO, O, H, and OH. Although several questions still remains, such as the relative contribution of $\text{CO}+\text{O}$ (Roser et al. 2001) and $\text{CO}+\text{OH}$ (Zins et al. 2011), and whether the reaction involves HOCO (Ioppolo et al. 2011), it is clear that water is formed on grains at the same time as CO_2 via reactions with hydrogen: $\text{O}+\text{H}\rightarrow\text{OH}$, $\text{OH}+\text{H}\rightarrow\text{H}_2\text{O}$. The experimental results and the temperature tracing method proposed in this study mostly apply to the CO_2 that is formed together with water by thermal processes. The second category of CO_2 formation mechanism involves energetic processing of the pure CO in the top layers of the ice mantle. Laboratory experiments have shown that CO_2 can be formed by the bombardment of analogues of cosmic rays with CO ice (Gerakines & Moore 2001; Loeffler et al. 2005; Jamieson et al. 2006). However, other molecules that should have also been produced in the energetic processing of CO, such as C_3O_2 (Jamieson et al. 2006), were not observed in the same sightline as CO_2 (Pontoppidan et al. 2008). The reason why a fraction of CO_2 is in CO-rich environment is still puzzling. If cosmic ray bombardment is important for CO_2 formation, the compaction of the ASW and the segregation of CO_2 from $\text{CO}_2:\text{H}_2\text{O}$ mixtures should also be affected by cosmic rays. It would be less relevant to characterize the ice mantle by temperature than to use the fluence of cosmic rays. In any case, the use of CO_2 segregation or $^{13}\text{CO}_2$ to trace the temperature history of the ice mantle is only valid under the assumption that

cosmic ray irradiation is not the dominant mechanism for CO₂ formation.

5. SUMMARY

We made measurements in the laboratory of infrared absorption features of CO₂:H₂O ices with different mixing ratios, at different temperatures, and subjected to thermal cycles in order to elucidate the thermal history of ices observed towards YSOs with ISO-SWS (Boogert et al. 2000). We found that at a CO₂:H₂O concentration below 23%, there is no formation of pure crystalline CO₂. Thus, looking at pure crystalline CO₂ alone is not a good proxy for establishing the thermal history of ices. We found that the ν_3 feature of ¹³CO₂

does not suffer from this threshold concentration dependence, and its peak position and linewidth, together with the pure crystalline feature of ¹²CO₂, can be used to infer the temperature history of ices near YSOs. Data such as the ones presented here will help to characterize the segregation status and thermal history of ices in upcoming JWST observations with an extended range in the IR spectrum, and improved sensitivity and spectral resolution.

ACKNOWLEDGEMENTS

We thank Francis Toriello for technical assistance. This research was supported by NSF Astronomy & Astrophysics Research Grant #1615897.

APPENDIX

A. DEPOSITION OF GASES

CO₂ gas and water vapor were deposited onto the sample through background deposition using two UHV precision leak valves activated by two stepper motors controlled by a LabVIEW program. For the deposition of a single molecular species, the program first measures the base pressure of the chamber, and then calculates the target partial pressure based on a user set deposition rate. The pressure readings from the hot cathode ion gauge is corrected for the gas species in the LabVIEW program. A PID control loop is used to maintain the pressure at the target value. In the deposition of CO₂, it takes about 20 seconds for the pressure to stabilize at the set value. The ice thickness during deposition is calculated by the program in real time. When the thickness reaches the setpoint, the leak valve is closed quickly. Even after the valve is closed, the residual gas in the chamber continues to being deposited on the sample, until it is pumped out. We correct for the additional amount deposited from the residual gas by closing the valve slight before the target thickness is reached. The exact offset thickness is calculated from the deposition pressure and the pumping speed. After this correction, in the deposition of CO₂, the *relative* uncertainty of thickness measured by the integration of pressure over time is usually less than 0.1%. For water deposition, the uncertainty is larger (1%) because of the difficulty in maintaining a stable water inlet pressure in the gas manifold.

In CO₂:H₂O co-depositions, because the ion gauge can only measure the total pressure but not the partial pressure of each gas, we start with the deposition of one gas. CO₂ is deposited first because it is easier to control its deposition. Within 20 seconds of introducing CO₂, the deposition rate is already stable. We tested the stability of pressure by fixing the valve position after 20 seconds, and found that the pressure does not change over time. The same is not true for water because of the instability of inlet pressure. After finding out the stable valve position for CO₂, we stop the PID loop for the CO₂ valve and fix the valve position. We then use a PID loop for the water leak valve to obtain a stable pressure during co-deposition. When the set time is reached, both leak valves are closed immediately. For the co-depositions in this study, the deposition is over 25 minutes, and therefore the uncertainty in CO₂ amount is about 20 seconds over 25 minutes, which is about 1%.

The impingement rate (*IPR*), which is the number of molecules deposited per unit surface area per unit time, is calculated as follows:

$$IPR = \frac{P}{\sqrt{2\pi m k_B T}} \quad (A1)$$

where P is the chamber pressure after correction for the ion gauge gas specific ionization cross-section, m is the mass of gas molecule, and T is the gas temperature (assumed to be room temperature), k_B is the Boltzmann constant. It is assumed that the sticking of both CO₂ and H₂O are unity at 10 K (He et al. 2016), and the pressure in the vacuum chamber is uniform. This is a fair assumption, because the leak valves opening does not face the sample or cold head directly. The impingement rate can be converted to the unit of monolayer per second (ML/s) by assuming 1 ML = 10¹⁵ cm⁻². The absolute uncertainty of deposition is mostly due to the uncertainty in pressure measurement, and can be as high as 30%, as this is the accuracy of a typical hot cathode ion gauge. In the experiments, the uncertainty in

mixing ratio of the $\text{CO}_2\text{:H}_2\text{O}$ mixtures is governed by the relative uncertainty, while that of the total thickness of the mixture is governed by the absolute uncertainty.

REFERENCES

- Baratta, G. A., & Palumbo, M. E. 2017, *A&A*, 608, A81, doi: [10.1051/0004-6361/201730945](https://doi.org/10.1051/0004-6361/201730945)
- Bergin, E. A., Melnick, G. J., Gerakines, P. A., Neufeld, D. A., & Whittet, D. C. B. 2005, *ApJL*, 627, L33, doi: [10.1086/431932](https://doi.org/10.1086/431932)
- Boogert, A. C. A., Gerakines, P. A., & Whittet, D. C. B. 2015, *ARA&A*, 53, 541, doi: [10.1146/annurev-astro-082214-122348](https://doi.org/10.1146/annurev-astro-082214-122348)
- Boogert, A. C. A., Ehrenfreund, P., Gerakines, P. A., et al. 2000, *A&A*, 353, 349
- Boogert, A. C. A., Huard, T. L., Cook, A. M., et al. 2011, *ApJ*, 729, 92, doi: [10.1088/0004-637X/729/2/92](https://doi.org/10.1088/0004-637X/729/2/92)
- Charnley, S. B., Tielens, A. G. G. M., & Millar, T. J. 1992, *ApJ*, 399, L71, doi: [10.1086/186609](https://doi.org/10.1086/186609)
- Cooke, I. R., Fayolle, E. C., & Öberg, K. I. 2016, *ApJ*, 832, 5, doi: [10.3847/0004-637X/832/1/5](https://doi.org/10.3847/0004-637X/832/1/5)
- Ehrenfreund, P., Kerkhof, O., Schutte, W. A., et al. 1999, *A&A*, 350, 240
- Gerakines, P. A., & Moore, M. H. 2001, *Icarus*, 154, 372, doi: [10.1006/icar.2001.6711](https://doi.org/10.1006/icar.2001.6711)
- Gerakines, P. A., Whittet, D. C. B., Ehrenfreund, P., et al. 1999, *ApJ*, 522, 357, doi: [10.1086/307611](https://doi.org/10.1086/307611)
- Hama, T., & Watanabe, N. 2013, *Chemical Reviews*, 113, 8783, doi: [10.1021/cr4000978](https://doi.org/10.1021/cr4000978)
- He, J., Acharyya, K., & Vidali, G. 2016, *ApJ*, 823, 56, doi: [10.3847/0004-637X/823/1/56](https://doi.org/10.3847/0004-637X/823/1/56)
- He, J., Emtiaz, S., & Vidali, G. 2018, *ArXiv e-prints*, arXiv:1806.06980. <https://arxiv.org/abs/1806.06980>
- He, J., Emtiaz, S. M., & Vidali, G. 2017, *ApJ*, 837, 65, doi: [10.3847/1538-4357/aa5f52](https://doi.org/10.3847/1538-4357/aa5f52)
- He, J., & Vidali, G. 2018, *MNRAS*, 473, 860, doi: [10.1093/mnras/stx2412](https://doi.org/10.1093/mnras/stx2412)
- Hodyss, R., Johnson, P. V., Orzechowska, G. E., Goguen, J. D., & Kanik, I. 2008, *Icarus*, 194, 836, doi: [10.1016/j.icarus.2007.10.005](https://doi.org/10.1016/j.icarus.2007.10.005)
- Ioppolo, S., Sangiorgio, I., Baratta, G. A., & Palumbo, M. E. 2013, *A&A*, 554, A34, doi: [10.1051/0004-6361/201321176](https://doi.org/10.1051/0004-6361/201321176)
- Ioppolo, S., van Boheemen, Y., Cuppen, H. M., van Dishoeck, E. F., & Linnartz, H. 2011, *MNRAS*, 413, 2281, doi: [10.1111/j.1365-2966.2011.18306.x](https://doi.org/10.1111/j.1365-2966.2011.18306.x)
- Isokoski, K., Poteet, C. A., & Linnartz, H. 2013, *A&A*, 555, A85, doi: [10.1051/0004-6361/201321517](https://doi.org/10.1051/0004-6361/201321517)
- Jamieson, C. S., Mebel, A. M., & Kaiser, R. I. 2006, *ApJS*, 163, 184, doi: [10.1086/499245](https://doi.org/10.1086/499245)
- Keane, J. V., Boogert, A. C. A., Tielens, A. G. G. M., Ehrenfreund, P., & Schutte, W. A. 2001, *A&A*, 375, L43, doi: [10.1051/0004-6361:20010977](https://doi.org/10.1051/0004-6361:20010977)
- Loeffler, M. J., Baratta, G. A., Palumbo, M. E., Strazzulla, G., & Baragiola, R. A. 2005, *A&A*, 435, 587, doi: [10.1051/0004-6361:20042256](https://doi.org/10.1051/0004-6361:20042256)
- Mitchell, G. F., Maillard, J.-P., Allen, M., Beer, R., & Belcourt, K. 1990, *ApJ*, 363, 554, doi: [10.1086/169365](https://doi.org/10.1086/169365)
- Noble, J. A., Fraser, H. J., Aikawa, Y., Pontoppidan, K. M., & Sakon, I. 2013, *ApJ*, 775, 85, doi: [10.1088/0004-637X/775/2/85](https://doi.org/10.1088/0004-637X/775/2/85)
- Nummelin, A., Whittet, D. C. B., Gibb, E. L., Gerakines, P. A., & Chiar, J. E. 2001, *ApJ*, 558, 185, doi: [10.1086/322480](https://doi.org/10.1086/322480)
- Öberg, K. I., Fayolle, E. C., Cuppen, H. M., van Dishoeck, E. F., & Linnartz, H. 2009, *A&A*, 505, 183, doi: [10.1051/0004-6361/200912464](https://doi.org/10.1051/0004-6361/200912464)
- Pontoppidan, K. M., Fraser, H. J., Dartois, E., et al. 2003, *A&A*, 408, 981, doi: [10.1051/0004-6361:20031030](https://doi.org/10.1051/0004-6361:20031030)
- Pontoppidan, K. M., Boogert, A. C. A., Fraser, H. J., et al. 2008, *ApJ*, 678, 1005, doi: [10.1086/533431](https://doi.org/10.1086/533431)
- Qasim, D., Chuang, K. J., Fedoseev, G., et al. 2018, *A&A*, 612, A83, doi: [10.1051/0004-6361/201732355](https://doi.org/10.1051/0004-6361/201732355)
- Roser, J. E., Vidali, G., Manicò, G., & Pirronello, V. 2001, *ApJ*, 555, L61, doi: [10.1086/321732](https://doi.org/10.1086/321732)
- Smith, R. S., Huang, C., Wong, E. K. L., & Kay, B. D. 1997, *PhRvL*, 79, 909, doi: [10.1103/PhysRevLett.79.909](https://doi.org/10.1103/PhysRevLett.79.909)
- van der Tak, F. F. S., van Dishoeck, E. F., Evans, Neal J., I., & Blake, G. A. 2000, *ApJ*, 537, 283, doi: [10.1086/309011](https://doi.org/10.1086/309011)
- Vandenbussche, B., Ehrenfreund, P., Boogert, A. C. A., et al. 1999, *A&A*, 346, L57
- Whittet, D. C. B., Cook, A. M., Chiar, J. E., et al. 2009, *ApJ*, 695, 94, doi: [10.1088/0004-637X/695/1/94](https://doi.org/10.1088/0004-637X/695/1/94)
- Yamagishi, M., Kaneda, H., Ishihara, D., et al. 2015, *ApJ*, 807, 29, doi: [10.1088/0004-637X/807/1/29](https://doi.org/10.1088/0004-637X/807/1/29)
- Zins, E.-L., Joshi, P. R., & Krim, L. 2011, *ApJ*, 738, 175, doi: [10.1088/0004-637X/738/2/175](https://doi.org/10.1088/0004-637X/738/2/175)